

Observation of Griffiths-like phase in the quaternary Heusler compound NiFeTiSn

Snehashish Chatterjee, Saurav Giri, Subham Majumdar*
*School of Physical Sciences, Indian Association for the Cultivation of Science,
2A & B Raja S. C. Mullick Road, Jadavpur, Kolkata 700032, India*

Prabir Dutta
Jawaharlal Nehru Centre for Advanced Scientific Research, Jakkur, Bangalore, 560064, India

Pintu Singha, Aritra Banerjee
Department of Physics, University of Calcutta, Kolkata 700 009, INDIA

The quaternary Heusler compound NiFeTiSn can be considered to be derived from the exotic pseudogap-compound Fe₂TiSn by the replacement of one Fe atom by Ni. In contrast to Fe₂TiSn, which shows a disorder induced ferromagnetic phase, the ground state of NiFeTiSn is antiferromagnetic with the signature of spin canting. Interestingly, NiFeTiSn shows a Griffiths-like phase characterized by isolated ferromagnetic clusters before attaining the antiferromagnetic state. The Griffiths-like phase is possibly associated with the antisite disorder between Fe and Ti sites as evident from our powder X-ray diffraction study. The compound also shows rather unusual temperature dependence of resistivity, which can be accounted by the prevailing structural disorder in the system. NiFeTiSn turned out to be a rare example where Griffiths-like phase is observed in a semiconducting 3d transition metal based intermetallic compound with antiferromagnetic ground state.

I. INTRODUCTION

In recent times, transition metal based Heusler compounds and alloys [1] are in the limelight of active research by virtue of their diverse and novel electronic properties, which include half-metallic ferromagnetism, spin-gapless semiconductivity, Weyl semimetallicity, magnetic shape memory effect, high Seebeck effect, magneto- and baro-caloric effects, unconventional superconductivity, anomalous Hall effect and so on [2–4]. Among others, Fe₂TiSn deserves a special mention in the Heusler family due to its fascinating electronic and magnetic properties. First principle density functional theory (DFT) based calculation indicates the compound to have a non-magnetic ground state with a pseudogap at the Fermi level (E_F) [5]. The number of valence electrons (Z_t) is 24 in Fe₂TiSn, which implies zero moment according to the Slater-Pauling rule [6]. However, actual experimental measurement indicates that the compound is a weak ferromagnet with Curie temperature (T_C) close to 260 K and saturation moment $0.2 \mu_B/\text{f.u.}$ [7]. The possible origin of ferromagnetism is ascribed to the antisite disorder between Fe and Ti sites, a phenomenon which is very common among Heusler compositions. Initial analysis of the low-temperature heat capacity and the resistivity data led to the conclusion that the compound was a heavy fermion [5]. Optical conductivity measurements, however, shows a simple Drude-like response of free carriers ruling out the Kondo or heavy fermion like state [5, 8]. The low temperature anomaly in Fe₂TiSn is believed to arise from clustering of atoms, which is also in accordance with the picture of disorder induced ferromagnetism in the

system. Notably, the compound also shows large positive Seebeck coefficient at room temperature.

Fully ordered Fe₂TiSn crystallizes in the cubic L2₁ structure with space group $Fm\bar{3}m$, where Fe atoms occupy 8c (1/4, 1/4, 1/4) Wyckoff position. In case of an L2₁ full Heusler compound with general formula X₂YZ, the replacement of one X atom with a different transition metal (X') leads to a change in structural symmetry. The resultant compound (XX'YZ) retains the cubic symmetry but attains a different space group, $F\bar{4}3m$. The study of such quaternary Heusler compounds have accelerated drastically in last two decades because of their possible application as a spin-polarized material in spintronics (CoFeMnGa, CoFeMnGe, CoMnCrAl) [9–12]. Apart from their half metallic character, some of the quaternary compounds, such as CoFeMnSi, CoFeCrGa [13, 14], are found to be spin-gapless-semiconductors.

Considering rich physics associated with the full Heusler Fe₂TiSn, it might be tempting to study the quaternary Heusler compound derived from it. There are previous reports on doping at the Fe site, however, a detailed study on the quaternary derivative is lacking. It is already known that Ni₂TiSn is a Pauli paramagnet with vanishing local moment at the Ni site [15]. Therefore, it is worth studying the quaternary compound NiFeTiSn, where one Fe site is diluted by a Ni atom. Such substitution will not only reduce the Fe concentration, it will also change the local crystallographic environment of Fe due to the change in space group.

The degree of antisite disorder depends on the atomic radii of the constituent metals, and it is likely to differ in case of NiFeTiSn. In the previous work on Fe_{2-x}M_xTiSn (M = Ni, Co), superparamagnetic-like state has been predicted [16]. Also, doping is found to destroy the pseudogap at the E_F . Our present study on NiFeTiSn indicates an antiferromagnetic (AFM)-like state at very

* sspsm2@iacs.res.in

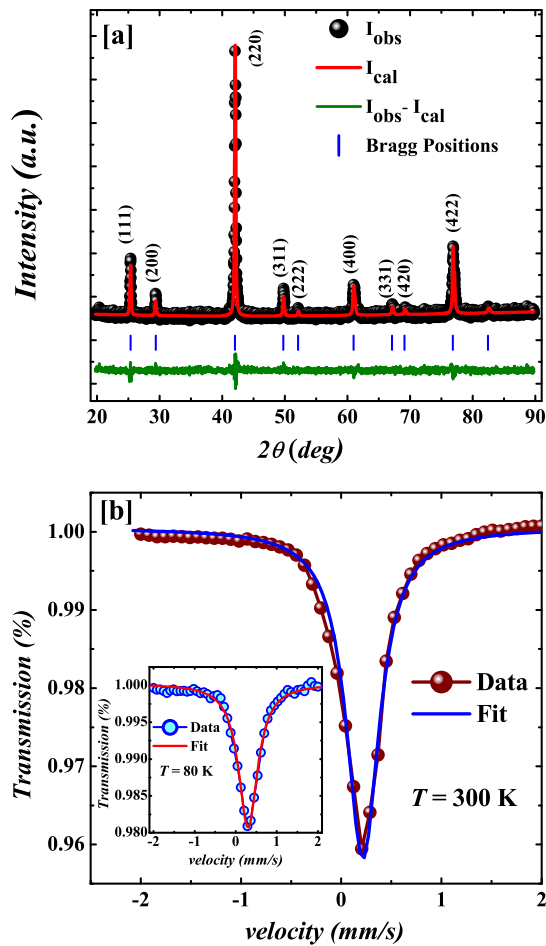


FIG. 1. (a) shows the powder X-ray diffraction pattern of NiFeTiSn (data points) at room temperature using Cu K_{α} radiation. The solid line is the Rietveld refinement fit to the data. (b) shows the Mössbauer spectrum of NiFeTiSn recorded at room temperature. The 80 K spectrum is shown in the inset.

low temperature (below about 7 K), which is in sharp contrast with the FM state reported for Fe_2TiSn . None the less, NiFeTiSn shows a non-Curie-Weiss-like state below about 275 K indicating the presence of short range magnetic correlations. Our investigations suggest that this state with short range magnetic correlations complies with the properties of the Griffiths phase (GP). In GP, the magnetic correlation does not vanish immediately above the long range ordering temperature, but it continues to exist up to a higher temperature [17–21]. In systems having ordered magnetic ground state, GP occurs due to the percolative nature of the distribution of short-range ferromagnetic (FM) clusters developed much above the ordering temperature in the magnetically disordered paramagnetic (PM) regime.

Magnetic materials, in presence of certain degree of disorder, can give rise to this remarkable GP-like magnetic

state. In majority of the cases, the GP is followed by a long range FM order at low temperature. The occurrence of GP in the AFM compounds are mostly reported in pnictides, manganites, perovskites [22–27] and few other rare-earth intermetallic alloys [28, 30, 31]. On the contrary, NiFeTiSn is a transition metal based intermetallic system with rather simple cubic structure. Our careful investigation and analyses indicate that the ground state of NiFeTiSn can better be described by a canted AFM one. In addition, the compound shows negative temperature coefficient of resistivity with rather unusual temperature dependence.

II. EXPERIMENTAL DETAILS

Polycrystalline NiFeTiSn was prepared using the stoichiometric ratio of the constituent elements by arc melting procedure in an inert argon atmosphere followed by annealing at 800°C for 3 days. Powder X-ray diffraction (PXRD) was performed at room temperature and the crystallographic structure was analysed using the Rietveld refinement technique with MAUD software package [32]. Magnetic measurements were carried out with the help of a commercial Quantum Design SQUID-VSM. The resistivity (ρ) was measured on a cryogen-free high magnetic field system (Cryogenic Ltd., U.K.) between 5–300 K. Thermoelectric measurements were carried out in the temperature range of 10 K–300 K using the differential technique. Heat capacity was measured using a Quantum Design physical properties measurement system.

To confirm the chemical composition of the sample, we performed a semi-quantitative Energy Dispersive X-Ray (EDX) analysis over multiple areas of the samples, and the average composition from the EDX analysis is found to be $\text{Ni}_{25.1}\text{Fe}_{23.6}\text{Ti}_{24.8}\text{Sn}_{26.6}$. From the obtained value, the equiatomic quaternary compound can be considered to be stoichiometric within the accuracy (2–5% [33]) of the EDX technique. ^{57}Fe Mössbauer spectra were recorded using an alternating constant WissEl Mössbauer spectrometer. The system operates in a horizontal transmission geometry with source, absorber and detector in a linear arrangement. Isomer shifts were measured with reference to α -iron metal foil at the same temperatures. Normos-A Mössbauer Fit program was used to fit the experimental data.

III. RESULTS

A. Powder X-ray Diffraction

Room temperature powder X-ray diffraction pattern for the compound NiFeTiSn is shown in Fig 1 (a). From the observed reflections and subsequent refinements, the sample is found to crystallize in the cubic Y-II type structure without any impurity phases. In this structure, Ni,

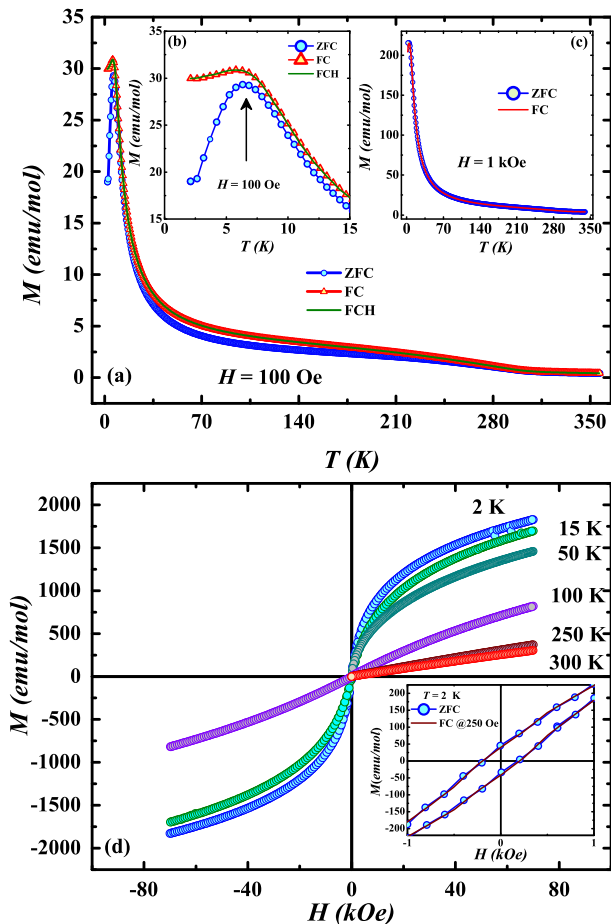


FIG. 2. (a) Magnetisation versus temperature plots in zero-field-cooled (ZFC), field-cooled (FC) and field-cooled-heating (FCH) protocols for NiFeTiSn measured under 100 Oe of magnetic field. (b) shows an enlarged view of the low temperature data highlighting the antiferromagnetic transition. (c) shows $M(T)$ for $H = 1$ kOe. (d) shows the isothermal magnetisation curves recorded at different constant temperatures. Inset shows an enlarged view of $M(H)$ at $T = 2$ K recorded in ZFC and FC condition.

Fe, Ti and Sn occupy the lattice sites $4b(1/2, 1/2, 1/2)$, $4d(3/4, 3/4, 3/4)$, $4c(1/4, 1/4, 1/4)$ and $4a(0,0,0)$ respectively [34, 35]. Both the superlattice reflection (111) and (200) are found to be present, indicating a predominantly ordered structure. However, for an ideal Y-type structure, the intensity of (111) and (200) in general remains the same. The reduction of (200) peak intensity in comparison to (111) peak ($I_{111}/I_{200} \sim 1.7$) might be due to the existence of antisite disorder in the studied sample. The cubic lattice parameter obtained from the refinement is found to be 6.070 \AA .

It is important to obtain a quantitative idea of the degree of disorder from the intensities of the diffraction peaks. A rough estimation of the degree of site ordering of the constituent atoms can be made by calculating the quantities $p = I_{200}/I_{220}$ and $q = I_{111}/I_{220}$, where I_{hkl} is the intensity of the (hkl) line in the PXRD pattern. The

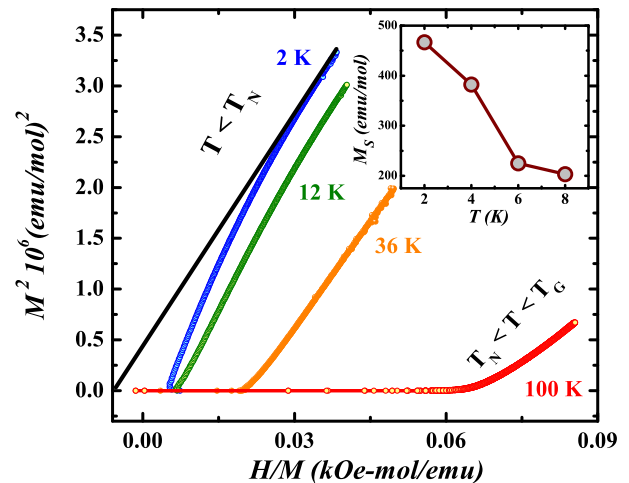


FIG. 3. Main panel presents the Arrot plot (M^2 vs H/M) of the sample recorded at different temperatures. Inset: Variation of spontaneous magnetisation (M_S) with T below T_N .

order parameters, σ and α are given by, $\sigma^2 = q_{obs}/q_{fit}$ and $\sigma^2(1-2\alpha)^2 = p_{obs}/p_{fit}$ [11]. Here the subscripts *obs* and *fit* correspond to the experimentally observed and the fitted values respectively. The fitted intensities are obtained from the Reitveld refinement without considering any site disorder. For an ideally ordered system, $\sigma = 1$ and $\alpha = 0$, and for fully B2 disordered case, $\sigma = 1$ and $\alpha = 0.5$. We get, $\sigma = 1.08$ and $\alpha = 0.1$ for NiFeTiSn. This indicates the presence of disorder (Fe-Ti antisite disorder) in case of NiFeTiSn.

Mössbauer spectra for NiFeTiSn [see fig 1(b)] recorded at both 300 K and 80 K exhibit singlet pattern, which indicates that local electric field at Fe site in the compound is symmetric. These singlet Mössbauer peaks at 300 and 80 K are well fitted with single Lorentzian function [36]. The Isomer shift is also found to be slightly higher at low temperature [0.24 mm/s (300 K) and 0.28 mm/s (80 K)].

B. Magnetisation

Temperature (T) variation of magnetisation (M) recorded for zero-field-cooled (ZFC), field-cooled (FC) and field-cooled heating (FCH) conditions under the magnetic fields, $H = 100$ Oe and $H = 1$ kOe are shown in fig. 2(a),(c). Both ZFC and FC data are characterized by a peak around 7 K indicating an AFM-like transition (see fig. 2(b)). More accurate value of the Néel temperature is obtained from the minimum of dM/dT versus T data, which is $T_N = 11$ K. ZFC and FC curves are found to bifurcate from each other from around $T_{irr} = 270$ K, which is much higher than T_N . There is a broad shoulder occurring around 250 K, and on further cooling, M increases with T . This thermo-magnetic irreversibility well above T_N and the presence of broad shoulder-like feature

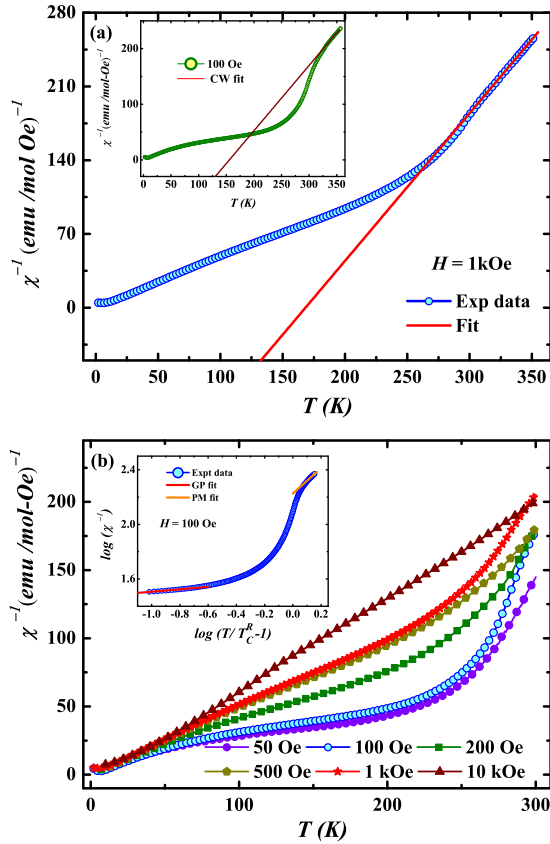


FIG. 4. (a) Inverse susceptibility versus temperature data recorded under $H = 1$ kOe. The inset shows the same data measured under 100 Oe. (b) shows inverse susceptibility data measured in different values of the applied field. Inset shows the log-log plot of inverse susceptibility as a function of $(T/T_C^R - 1)$.

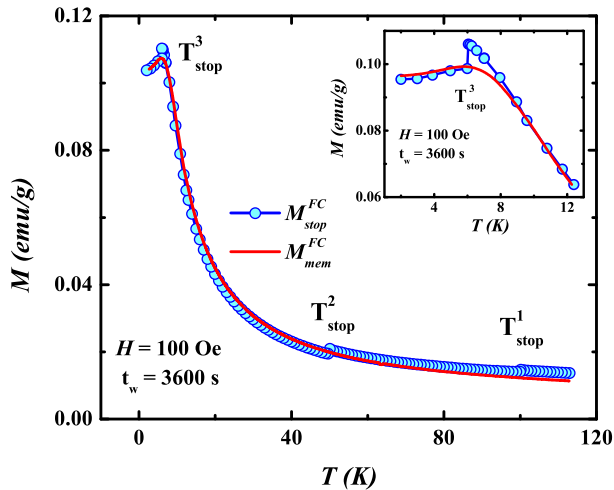


FIG. 5. Field-cooled-field-stop memory curves at three stopping temperatures, $T_{stop} = 6, 50$ and 100 K. The inset shows an enlarged view of the low temperature data.

hint towards the existence of the short-range magnetic correlations in the backdrop of a PM phase [37]. Under $H = 1$ kOe, the low- T bifurcation between ZFC and FC curves becomes weak and shifts to lower- T and the T_{irr} almost vanishes.

Fig. 2(d) shows the isothermal M versus H curves recorded at different constant temperatures in the ZFC condition ($T = 2, 15, 100, 250$ and 300 K), between $H = \pm 70$ kOe. The isotherms below 250 K follow an ‘S’-shaped nature with no saturation tendency even at $H = 70$ kOe. The non-linear nature of the $M(H)$ curves at temperatures well above T_N [see 100 and 50 K isotherms in fig. 2(d)] reaffirms the existence of the short-range correlations. Inset of fig. 2(d) shows an enlarged view of $M(H)$ at $T = 2$ K recorded in ZFC and FC conditions under $H = 250$ Oe, indicating small coercive field close to 200 Oe and the absence of any exchange-bias in the compound.

Figure 3 shows the Arrot (M^2 versus H/M) plot at few constant temperatures [38]. The curves are quasi-linear at higher values of H/M for all temperatures above and below T_N . The linear extrapolation of the high- H data shows positive intercept on the M^2 axis for the isotherms recorded below T_N . Such positive values of M^2 (below T_N), indicates the presence of spontaneous magnetisation, M_S (as obtained from the square root of M^2). However, such positive intercept is absent for the data recorded above T_N . This indicates that there exists a finite M_S only below T_N , and possibly the system has a canted antiferromagnetic ground state.

In the main panel of fig. 4(a), we have plotted inverse susceptibility ($\chi^{-1} = H/M$) as a function of T . A linear region is observed between 310-360 K, and we have fitted this part using the Curie-Weiss (CW) law, $\chi = C/(T - \theta_p)$, where C is the Curie constant, θ_p is the paramagnetic Curie-Weiss temperature. From the fitting, we obtain the effective paramagnetic moment, μ_{eff} to be $2.48 \mu_B$, and $\theta_p = 128$ K. The observed large positive value of θ_p indicates the presence of dominant FM correlations in the system.

To shed some light on the observed behaviour, we have plotted χ^{-1} versus T data over a wide range of temperatures. A strong downward deviation from the CW law is observed from below about 300 K for the 100 Oe data (inset of fig. 4(a)). This downward behaviour of χ^{-1} decreases with increasing H and disappears for $H = 10$ kOe [fig. 4(b)]. The observation of a downward deviation in the χ^{-1} versus T curve at temperatures much higher than magnetic ordering temperature (in this case T_N) is a hallmark of the presence of the Griffiths-like phase [37, 39, 40]. The GP is characterized by the appearance of the finite size FM clusters in the backdrop of a PM phase well above the long range order sets in [41, 42]. χ of the system fails to follow the typical Curie-Weiss law above T_N up to a certain critical temperature known as Griffiths temperature (T_{GP}). However, with increasing H , the downturn in the χ^{-1} vs T data softens and becomes gradually indistinguishable

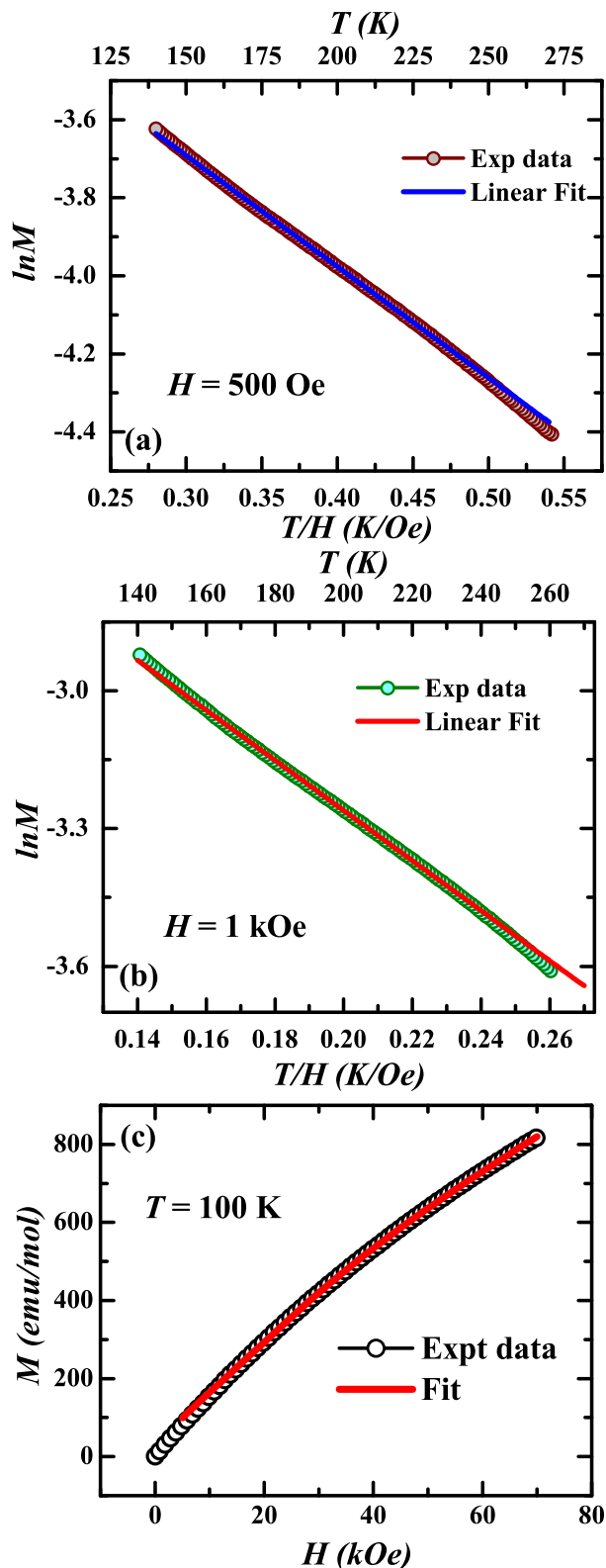


FIG. 6. (a) and (b) shows $\log M$ versus T/H plot of NiFeTiSn under the applied field of $H = 500$ Oe and 1 kOe. The solid line is the best linear fit using the relation 2. (c) shows Magnetisation as a function of field at $T = 100$ K following a power-law behaviour.

from the high- T paramagnetic regime [30, 43]. The application of a sufficiently high H polarizes the spin on the outside part of the clusters, leading to the suppression of the signature of GP in the χ^{-1} vs T data [30, 37]. The cluster-like FM component is masked at higher- H by the linear increase of the PM contribution of the matrix [42].

It is known that the inverse susceptibility in the GP obeys a power law behaviour characterized by an exponent (λ) [17, 23],

$$\chi^{-1} \propto (T - T_0^R)^{(1-\lambda)} \quad (1)$$

where, $0 < \lambda < 1$ for $T_N < T < T_{GP}$. In the PM phase, $\lambda \rightarrow 0$, and eqn. 1 turns into usual CW law. T_0^R can be obtained from the paramagnetic phase by setting $\lambda \sim 0$, which is close to the PM Curie temperature. We have plotted $\log(\chi^{-1})$ against $\log(T/T_0^R - 1)$ [inset of fig. 4(b)] and the value of λ is obtained from the slope of the linear fit using equation 1 (solid red line fit). In PM and GP regions, the obtained values of λ are 0.006 and 0.91 respectively (using $T_0^R = 147$ K). Similar λ value is earlier reported for Heusler alloys $\text{Fe}_{2-x}\text{Mn}_x\text{CrAl}$ showing Griffiths-like behaviour [44]. A large difference between T_N and T_{GP} is observed in NiFeTiSn along with a value of λ close to unity in the GP regime. This signifies the strong deviation from the CW behaviour and point towards the robustness of the GP in this material. The deviation of $\chi^{-1}(T)$ from CW law prevails even for H as high as 10 kOe. This feature is also unusual compared to other systems where such deviation vanishes for $H \gtrsim 1$ kOe [22, 23].

Galitski *et.al.* [45] studied the GP in the dilute magnetic semiconductor in the light of magnetic polarons. The magnetisation in the GP is found to be weak and it follows a relation:

$$M(H, T) \propto \exp\left[-B\frac{T}{H}\right] \quad (2)$$

where, B is a constant. It is to be noted that eqn. 2 does not take into account the pinning effect between the magnetic clusters which is relevant in the low field regime. Hence, the $M(T)$ data measured at lower fields ($H = 50, 100$ and 200 Oe) cannot be fitted well using eqn 2 [46]. In figure 6(a,b) we have plotted $\log M$ versus T/H along with linear fit for $H = 500$ Oe and 1 kOe within the temperature range 160 - 220 K. The value of the constant B obtained from fitting is 28.4(3) and 54.5(4) Oe/K for $H = 500$ Oe and 1 kOe respectively, which are similar to the earlier reported values for other GP systems. [46, 47].

To confirm GP in NiFeTiSn, 100 K $M(H)$ isotherm has been plotted in figure 6(c). M is found to obey the predicted GP behaviour given by,

$$M(H) = M_0 + aH^\eta \quad (3)$$

where M_0 is the non-zero spontaneous magnetisation and η is an exponent [48, 49]. The best fit between 20 to

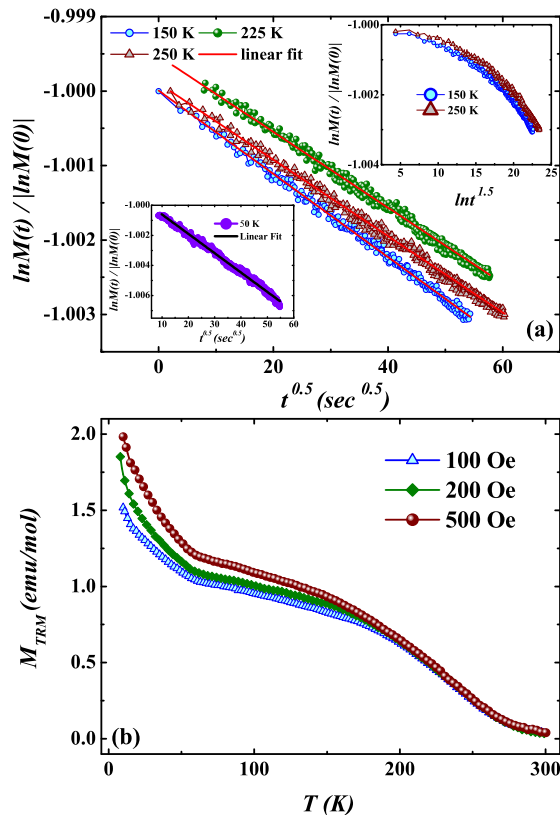


FIG. 7. (a) shows thermo-remnant magnetisation after the sample being cooled in different fields. (b) Magnetic relaxation measured in the field cooled state at different constant temperatures, where $\log M$ is plotted as a function of $t^{0.5}$. We have also plotted $\log M$ as function of $(\log t^{1.5})$ (upper inset of (b))

70 kOe yields the exponent η to be 0.78. This value of η is close to the value of λ obtained from eqn. 1, and such closeness of these two exponents is common in GP [50]. Most importantly, a power law variation of $M(H)$ curve (eqn. 3) is a clear deviation from the linear $M(H)$ behaviour expected in a pure PM region (CW law) [48, 51].

To get further idea of the nature of the magnetic state in NiFeTiSn, we performed field-cooled-field-stop memory (FCFS memory) measurement as shown in fig. 5 [52, 53]. Initially, the sample was cooled under $H = 100$ Oe from 300 to 2 K with intermediate stops at $T_{stop}^i = 6, 50$ and 100 K for $t_w = 3600$ s each. The magnetic field was turned off at T_{stop}^i which results in a step-like magnetization curve (M_{stop}^{FC}). After reaching 2 K, the sample was further heated in presence of $H = 100$ Oe without any stops (M_{mem}^{FC}) [see fig. 5]. Interestingly, the heating curve, M_{mem}^{FC} , does not show any anomaly at the stopping temperatures where the sample was allowed to stop during cooling. This points to the fact that no FC memory is present in the system, ruling out the possibility of a spin-glass or superparamagnetic state.

We further studied the thermoremanant magnetisation

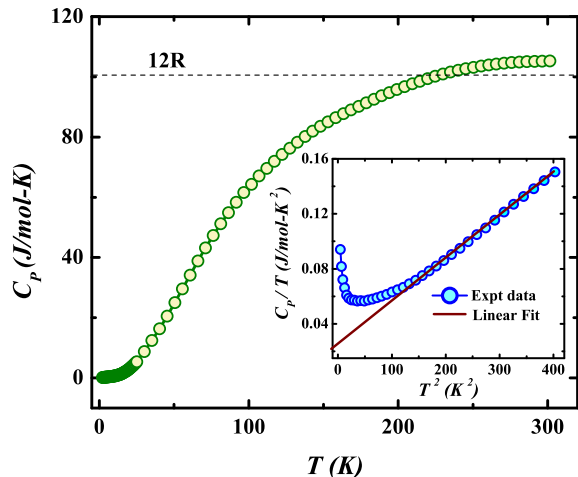


FIG. 8. Heat capacity as a function of temperature. The inset shows the low- T C_p versus T^2 plot and solid line is a linear fit to the data.

(TRM), M_{TRM} , to characterize the GP [40, 54]. The protocol involves cooling the sample from well above the magnetic transition temperature in the presence of cooling field, H_{cool} . The field is removed below T_N , and the magnetisation is measured while heating under $H = 0$. In the present case, this protocol was repeated for three different cooling fields, $H_{cool} = 100, 200$ and 500 Oe [fig 7(a).] The zero-field measurements have the advantage that the contributions from the paramagnetic susceptibility are suppressed compared to an in-field measurement. All the three curves (recorded in zero field while heating after being cooled in different values of H_{cool}) show sizeable TRM below 300 K. At temperature above about 210 K, these curves are practically indistinguishable. Below about 200 K, the curves start to diverge from each other and a hump-like feature is observed. On field cooling, the FM clusters of the GP are created favourably with the direction of H_{cool} . When the sample is heated from the lowest temperature after setting $H = 0$, the clusters remains pinned and provide us a remanent magnetisation. The TRM eventually disappears above a certain temperature when the GP is destroyed. The presence of TRM supports the existence of magnetic clusters in the material.

The short-range FM regions in the GP drastically influence the dynamics of the magnetic susceptibility. In the GP, the time required to reverse the effective spin of clusters would be larger, resulting in a non-exponential decay of the spin-auto correlation function [55]. For randomly diluted ferromagnets, this decay has been calculated to be of the form $\sim \exp(-Bt^{0.5})$ and $\sim \exp[-A \ln t^{(1.5)}]$ for 3D Heisenberg and Ising spin systems respectively [56]. Fig. 7(b) highlights the isothermal remanent magnetisation (IRM) data for NiFeTiSn within the GP regime (50, 150, 225, and 250 K). We cooled the sample from 300 K in presence of $H = 50$ Oe to a particular tempera-

ture of measurement, subsequently the time variation of M was recorded for 3600 s after switching off the magnetic field. Good linear fit is obtained for $\log M$ versus $t^{0.5}$ data for all the temperatures. The upper inset of fig. 7(b) presents the plot for $\log M$ versus $\log t^{1.5}$, and its non-linear nature rules out the Ising nature of the spins within the clusters. We can conclude that the interaction between spins in the GP regime are Heisenberg-like. The TRM and IRM measurements provide strong evidence in favour of the presence of FM clusters within the PM matrix [40, 55].

Fig. 8 shows the zero-field heat capacity (C_p) data measured between 2-300 K, where C_p decreases monotonically with decreasing T . C_p tends to saturate above 250 K and its value at 300 K is found to be $105 \text{ J mol}^{-1}\text{K}^{-1}$. This value is marginally higher than the classical Dulong-Petit value of $12R/\text{mol} = 99.8 \text{ J mol}^{-1}\text{K}^{-1}$ (R is the universal gas constant). Such deviation in $C_p(T)$ is a signature of phonon anharmonicity in presence of disorder [57, 58]. Notably, C_p does not show any λ -like anomaly at around T_N . However, C_p/T vs T^2 data show a shallow minimum below T_N (see inset), which possibly related to the AFM-like order in the system. The C_p/T vs T^2 varies linearly between $T = 12$ and 20 K, and the Sommerfeld coefficient γ obtained from this linear region is found to be $26 \text{ mJ mol}^{-1}\text{K}^{-2}$ [59]. This value is twice as high than the full Heusler Fe_2TiSn [5]. The absence of λ -like anomaly in the heat-capacity data is not uncommon among Heusler family of compounds [60, 61].

In many instances, spin glass are found to show a broad hump like feature in the heat capacity (C_p versus T). In our data, we rather observe a sharp rise in the C_p/T vs T^2 plot, which is not a standard feature of the glassy magnetic phase [61]. Such low- T upturn below T_N can be taken as an evidence for the onset of bulk magnetic ordering in the sample. Due to the presence of Griffiths-like short range correlation, a significant amount of magnetic entropy is already released when the sample is cooled down to T_N from 300 K. Such pre-existing magnetic correlation will effectively weaken the signature in C_p at T_N [62, 63].

C. Electrical Resistivity and Thermopower

The $\rho(T)$ behaviour of NiFeTiSn [see fig. 9(a)] is found to have a negative ($d\rho/dT < 0$) temperature coefficient of resistivity (TCR). $\rho(T)$ is also characterized by a sharp rise below 12 K. Several quaternary and half Heusler compounds, such as CoFeCrGa [14], CoFeMnSi, CrV-TiAl [64], YPdSb, LuNiSb [65], show negative TCR over a wide T -range. Interestingly, the nature of the $\rho(T)$ data above 20 K in NiFeTiSn is found to be rather unusual as compared to the common semiconducting materials. In a semiconductor, the carriers are thermally excited across an energy gap, and one generally finds an exponential (or sometimes stretched exponential) type of $\rho(T)$ data where the ρ versus T plot is convex upward. This has

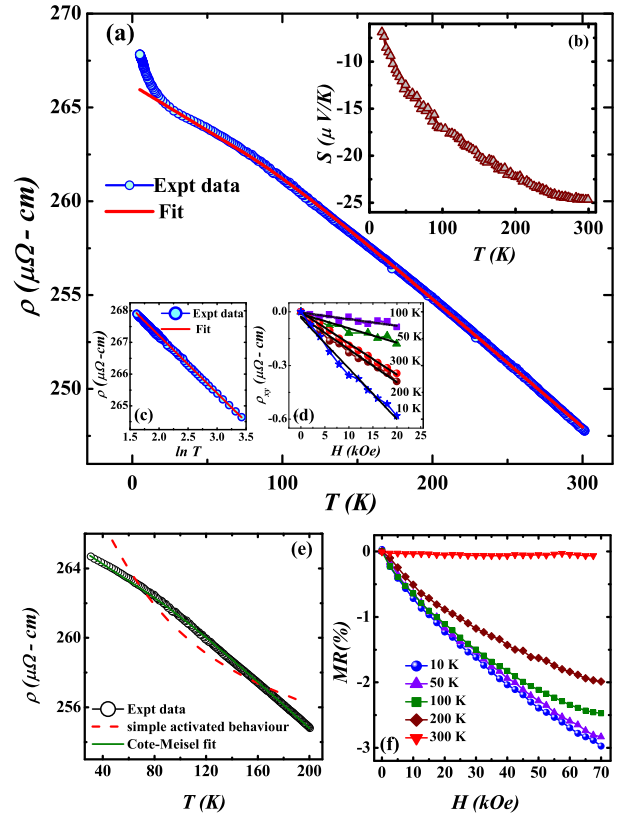


FIG. 9. (a) Resistivity as a function of temperature. (b) shows the T variation of thermopower. (c) presents the ρ vs $\ln T$ data in the range 5-50 K (d) presents ρ_{xy} vs H at different constant temperatures. (e) $\rho(T)$ data along with the fitting (black solid line) using the model proposed by Cote and Meisel (see eqn 4 in the text). The red dashed line shows the common activated behaviour (convex upward) (f) Magnetoresistance measured at different temperatures.

been exemplified by an exponential resistivity behaviour (red dashed line) in fig. 9(e). On the contrary, NiFeTiSn shows a concave upward nature, where the curvature is opposite to that of common semiconductors.

The negative TCR in disordered metallic systems is often considered in the framework of generalized Faber-Ziman theory for liquid metals and further extended for amorphous and crystalline solids by Cote and Meisel [65–70]. In this model, the resistivity of highly resistive metals can be expressed as

$$\rho(T) = \exp(-2\overline{W}(T))(\rho_0 + \Delta_{ep}) \quad (4)$$

where,

$$\overline{W}(T) = \frac{3h^2 < k^2 > T^2}{8\pi^2 m k_B \theta_D^3} \int_0^{\theta_D/T} \left[\frac{1}{e^z - 1} + \frac{1}{2} \right] z dz \quad (5)$$

Here, ρ_0 is the residual resistivity due to the scattering of electrons with static defects, and Δ_{ep} is the inelastic

electron-phonon interaction term. $2\overline{W}(T)$ is the Debye-Waller exponent averaged over all the scattering vectors k of the conduction electrons. In eqn. 5, m stands for the ionic mass, while h , k_B and θ_D are respectively Planck constant, Boltzmann constant and Debye temperature. For disordered metals with high value of ρ_0 , Δ_{ep} is negligible as compared to ρ_0 . Since $2\overline{W}(T)$ increases with increasing T , eqn. 4 will lead to a negative TCR. We have fitted eqn. 4 to the $\rho(T)$ data with an approximation that Δ_{ep} is negligible as compared to ρ_0 for NiFeTiSn. The fitting [fig 9(a)] converges well between 70 to 300 K and we obtain $\rho_0 = 270 \mu\Omega\text{-cm}$, $\langle k^2 \rangle = 5.88 \times 10^{21} \text{ m}^{-2}$ and $\theta_D = 327 \text{ K}$.

To explain the low- T upturn in $\rho(T)$, we have plotted the data (5-50 K) as a function of $\ln T$ [fig. 9 (c)]. A linear variation indicates the upturn to be logarithmic in nature. Such upturn may arise due to weak localization or Kondo effect [71].

Notably, NiFeTiSn presents a small ($\sim -3\%$) negative MR at $T = 10 \text{ K}$ as shown in fig. 9(f). With increasing T , the magnitude of the MR decreases and it is about -2% at 200 K. However, the MR turns negligible at 300 K. The finite negative MR at 200 K, which is well above the magnetic ordering temperature, is in line with the short range magnetic correlations.

T dependence of Seebeck coefficient (S) was measured for NiFeTiSn and shown fig. 9(b). The negative value of S indicates that electron is the dominant carrier. S increases with T following a quasilinear behaviour up to room temperature. The maximum value of $|S|$ is found to be around $25 \mu\text{V/K}$ at room temperature. The absolute value of S at 300 K for NiFeTiSn is comparable to that of potential thermoelectric Heusler alloys such as Fe_2VGa and Ru_2NbGa ($\sim 25 \mu\text{V/K}$) [72]. NiFeTiSn has appreciable value of thermoelectric power factor $\text{PF} = S^2/\rho$ of $2.5 \mu\text{W}\cdot\text{cm}^{-1}\cdot\text{K}^{-2}$ at 300 K. This value of PF is comparable to good thermoelectric materials such as semimetallic Ru_2NbGa and Ru_2NbAl [60, 73, 74]. We have also measured the transverse Hall resistivity (ρ_{xy}) and its variation with H is shown in fig. 9(d). We have calculated the values of carrier concentration (n) and Hall mobility (μ_H) at $T = 10, 300 \text{ K}$, and they are found to be $n = 2.3 \times 10^{21}, 2.2 \times 10^{21} \text{ cm}^{-3}$ and 10.2, 11.5 $\text{cm}^2/\text{V}\cdot\text{s}$ respectively. Negative Hall coefficient also supports the result obtained from $S(T)$ measurement, *i.e.*, electrons are the dominant carriers in NiFeTiSn. The μ_H obtained for NiFeTiSn is comparable to other reported Heusler compounds [75, 76].

IV. DISCUSSION

There are only limited number of reports for Griffiths-like phase in Heusler alloys and compounds. They include systems such as Fe_2VGa , Fe_2VAl and Fe_2CrAl -based alloys. The present NiFeTiSn is a quaternary Heusler compound, and to our knowledge, FeMnCrAl is the only other compound showing GP in this series [44].

However, unlike NiFeTiSn, FeMnCrAl has a long range FM ground state. The cusp like feature around 7 K both in the ZFC and FC magnetisation data indicates that the ground state is AFM-like in NiFeTiSn [fig. 2 (a)].

So far, most of the experimentally reported intermetallic GP compounds order ferromagnetically at low temperature [23, 30, 44], and AFM GP compounds are relatively lesser in number. The signature of GP above T_N is quite convincingly established from our study. The archetypal signature of GP is evident from the χ^{-1} versus T data, where we observe a strong downturn from linear Curie-Weiss law below T_{GP} ($\approx 275 \text{ K}$). We also observe a power law variation of inverse susceptibility ($\chi^{-1} \sim T^{1-\lambda}$), which is a common protocol to establish a GP. The magnetisation of NiFeTiSn also obeys the scaling law, $\ln M \sim -\frac{T}{H}$ roughly in the temperature range between T_N and T_{GP} .

Microscopically a GP is characterized by spatially isolated non-interacting FM clusters in a paramagnetic matrix. Therefore, it is pertinent to show that our compound is devoid of any long-range order between T_N and T_{GP} . If we extrapolate the high H/M Arrot plot data (above T_N) towards the origin [see fig. 3], they strike the ordinate at negative values of M^2 , indicating the lack of spontaneous magnetisation. Further proof opposing the long range ordered phase between T_N and T_{GP} is obtained from our Mössbauer spectra. The distinct singlet line obtained both at high- T (300 K) and low- T (80 K) confirms the lack of a long range magnetic order in these T range for NiFeTiSn. The Mössbauer line recorded at 80 K ($\gg T_N$) is found to be significantly wider than that of 300 K data. This increase in the width possibly indicates the growth of the short range FM clusters with decrease in T . Similar observation were reported in the Heusler compounds Fe_2VGa and Fe_2VAl [77, 78] and Eu-doped $\text{Ca}_3\text{Co}_2\text{O}_6$ [79].

The unexpected magnetic anomaly observed close to room temperature could also be associated to the existence of ferromagnetic impurity phase with a T_C close to room temperature. However, such possibility can be convincingly ruled out in light of the following evidences: (A) Lack of spontaneous magnetisation (for $T > T_N$) indicates the absence of long-range ferromagnetic ordering and thus excludes the possibility of the existence of a FM impurity phase. (B) The Mössbauer spectra have singlet line at 300 K and 80 K. The line is sharp and symmetric. Had there been any ferromagnetic impurity or ordering, one should see a splitting or broadening of the line. ^{57}Fe Mössbauer spectra is quite sensitive to any ordered impurity phase. For example, even 1% Fe (non-enriched) doping in BaTiO_3 can produce significant splitting of the singlet line [80]. However, in case of NiFeTiSn, we find the Mössbauer line which can be well fitted by a single Lorentzian function [see fig. 1(b)]. This certainly signifies that the sample does not order magnetically at least down to 80 K within the accuracy of the Mössbauer technique. The lack of magnetic order is the most important characteristics of a Griffiths-like phase and the

present data supports the presence of GP in the studied compound. (C) Careful observation and analysis of x-ray powder diffraction data for NiFeTiSn reveals the absence of any major impurity phase (within the accuracy limit of the experimental technique). All the peaks observed can be indexed to the cubic LiMgPdSn type Heusler structure [81]. (D) The nonexponential decay of M with time above T_N indicates isolated non-frustrated spin clusters [55] and it rules out long-range ordering of the FM impurity phase. Above all, χ and M follow the appropriate scaling laws of a GP as opposed to the behaviours of an FM state.

Magnetic relaxations measured in the GP-regime of the sample [see fig 7(a)] does not obey a simple exponential law. Instead, we observe $M(t)$ to follow $\exp[-\sqrt{\frac{t}{\tau}}]$ type of variation with time. Theoretical arguments indicate that such form of relaxation is a signature of Heisenberg type spin system within the FM clusters of the GP [18, 19]. As an example, REBaCo₄O₇ (RE = rare-earth) compounds show similar relaxation behavior, and the Heisenberg nature of the spin system is further verified by means of neutron scattering experiments [82].

NiFeTiSn has a simple cubic structure at room temperature and it does not show any change in its lattice symmetry as a function of temperature [16]. The full Heusler compound Fe₂TiSn is an important example where ferromagnetism originates from antisite disorder. Our PXRD analysis indicates about 17% antisite disorder between Ti and Fe sites. Such disorder can create isolated Fe-rich magnetic clusters leading to Griffiths-like phase. Interestingly, NiFeTiSn shows GP from 280 K, which is very close to the Curie temperature of Fe₂TiSn. DFT based calculations indicate small value of moment at the Ni site of the quaternary compounds NiFeTiZ (Z = P, As, Si, Ge) [83]. As compared to Fe₂TiSn, one Fe atom is replaced by Ni in NiFeTiSn, and this dilution of Fe atoms might be responsible for the lack of long range FM order developing around 260-280 K. Instead, isolated FM clusters are formed in the latter compound leading to Griffiths-like phase. It is worth noting that GP in Fe₂VGa and some of its dopants is also related to antisite disorder between Fe and V sites [84].

In the original conjecture laid down by Griffiths, the short range FM clusters in the GP can eventually lead to a long-range ordered FM ground state on lowering the temperature. However, the situation can be different if the ground state attains antiferromagnetism. There are numerous examples in the literature on such antiferromagnetic Griffiths-like phase, and the present NiFeTiSn is found to be a new addition to the list. The most pertinent question regarding the AFM GP is the nature of the magnetic ground state. In the literature, there are reports where the short range FM clusters continue to coexist with the long-range state at low temperature (example, Ca₃CoMnO₆ [85]). Such coexistence can give rise to spin glass or cluster glass like phase arising from the competition between FM clusters and the

AFM phase. For example, glassy magnetic phase is observed below T_N in the double perovskites La₂FeMnO₆ and Pr_{2- x} Sr _{x} CoMnO₆ [24, 25]. Many of these compounds also show exchange bias effect at low temperature, which is an evidence for magnetic inhomogeneity. On the contrary, electron spin resonance experiment categorically ruled out the presence of short range FM phase below T_N in the manganite Eu_{0.6}La_{0.4- x} Sr _{x} MnO₃ [39].

In a magnetic solid, GP can have different origins, such as quenched disorder (in manganites), phase separation, micro-twinning, competing intra and inter-layer magnetic interactions (in a quasi-two dimensional system), cluster formation in nano-sized materials and so on. Among intermetallics, GdSn₂ based alloys are also claimed to have GP along with AFM ground state. On the basis of x-ray powder diffraction coupled with the spin-polarized density functional calculations, Ghosh *et.al.* established a direct structural connection to GP in intermetallic GdM _{x} Sn_{2- δ} (M = Co, Ni, Cu; 0 < x < 1, δ = 0-0.22) [28, 29]. Griffiths-like phases are also reported in the magnetically disordered rare-earth based intermetallic compounds Tb₅Si₂Ge₂ and RE₅Si _{x} Ge_{4- x} series [28, 30, 31]. In this case, the occurrence of GP is microscopically associated with competing intra- and interlayer exchange interactions, due to their complex structure. In contrast, NiFeTiSn belongs to cubic Heusler series containing 3d transition metals and *sp* element only. The cubic structure is retained down to low temperature [16] and it is pretty much three dimensional in nature without having any chance for quasi-low dimensional magnetic correlation. Unlike manganites and cobaltites, the system is devoid of electronic phases separation. The phase separation due to structural transition, observed in Heusler based shape memory alloys, is also absent here as the system retains the cubic Heusler structure down to low temperature. Hence, it can be assumed that the structural correlation is not the reason for the formation of GP in the cubic NiFeTiSn. Rather, it is more likely that antisite disorder is the key driving force for the observed GP-like anomaly.

In case of NiFeTiSn, we failed to observe any signature of FCFS memory neither below nor above T_N , and a spin glass/superparamagnetic phase can be ruled out for the compound. The compound does not show any signature of exchange bias at 2 K (see inset of fig 2(d)), which also demonstrates that there is no major magnetic inhomogeneity below T_N . The χ^{-1} versus T data [fig. 4 (b)], measured at different H , converge at T_N . Had there been any FM cluster present below T_N , one would expect χ^{-1} to follow different paths depending upon H . These observations, apparently points that the GP ceases to exist below T_N in NiFeTiSn.

Nevertheless, the ground state of NiFeTiSn is not purely AFM as evident from the magnetic isotherms depicted in fig. 2(d). The $M - H$ curves below 50 K show ‘S’-like nature, and a finite coercivity of 200 Oe and a remanent magnetisation of 48 emu/mol are observed at 2 K [inset of fig. 2 (d)]. The finite coercivity undoubt-

edly indicates the presence of an ordered FM component below T_N , and the resultant magnetic structure is likely to be canted AFM type. The short range FM correlation present in the sample in the form of GP might be instrumental for spin canting when the sample attains a long-range order below T_N . It is to be noted that the value of spontaneous magnetisation obtained from the Arrot plot is quite small, which corresponds to the weak ferromagnetism below T_N due to spin canting [86, 87]. However, we also have to rule out the possibility of the sample being a simple ferrimagnet. In case of a ferrimagnet, there have to be two antiparallel sublattices with different magnetic moment values. Consequently, the net moment will be non-zero. For the present NiFeTiSn, there can be Ni and Fe sublattices. The band structure calculations of similar compounds such as NiFeTiZ (Z = P, Si, Ge, As) shows that the moment at the Fe site (m_{Fe}) is much larger than that of the Ni site (m_{Ni}) [83]. Therefore the net moment ($m = m_{\text{Fe}} - m_{\text{Ni}}$) will be significant. Since our data indicates very small value of M_S , the scenario for a ferrimagnetic state is improbable.

NiFeTiSn shows a negative thermal variation of ρ , but does not resemble a general activated behavior found in semiconductors. Rather $\rho(T)$ shows an unusual nature where the curve is *concave downwards*. Fe₂TiSn, on the other hand, shows metallic behaviour below about T_C , and shows negative temperature coefficient behaviour of resistivity ($d\rho(T)/dT < 0$) in the PM region [88]. The metallicity in Fe₂TiSn is believed to be connected to the long range FM order. Since NiFeTiSn does not order ferromagnetically at high temperature, it retains its neg-

ative temperature coefficient of resistivity down to low temperatures. The $\rho(T)$ data between T_{GP} and T_N can be fitted with Cote-Meisel model [67] for disordered systems. The scattering of conduction electrons with static site disorders and/or isolated magnetic clusters is possibly responsible for the rather unusual $\rho(T)$ variation in this temperature window. Interestingly, the Seebeck coefficient of NiFeTiSn is found to be negative as compared to the positive value in Fe₂TiSn, although the magnitudes of thermopower are comparable [76]. As shown in fig 9(b), the magnitude of S increases with increasing temperature following a quasilinear behavior up to room temperature. For heavily doped semiconductors (parabolic band, energy-independent scattering approximation) with degenerate character of electrons/holes, the magnitude of S generally increases monotonically with increasing T . [76, 89, 90].

In conclusion, we report an extensive investigation on the cubic Heusler compound NiFeTiSn by means of magnetic, Mössbauer, electrical and thermal transport properties measurements. The work establishes a Griffiths-like phase that exists over a wide range of temperature (15-275 K). The ground state of the compound is found to be canted AFM type in nature, and our work indicates that the FM clusters due to GP disappear with the advent of this canted AFM state below T_N .

ACKNOWLEDGMENT

SC wishes to thank UGC, India for his research fellowship. The work is supported by the grant from SERB, India with grant number EMR/008063.

-
- [1] Nanda B R K and Dasgupta I 2003 *J. Phys.: Condens. Matter* **15** 7307
- [2] Graf T, Felser C, Parkin S S P 2011 *Prog. Sol. Stat. Chem.* **39** 1
- [3] Zhu L J and Zhao J H 2017 *Sci. Rep.* **7** 42931
- [4] Huang L, Zhang Q, Yuan B, Lai X, Yan X and Ren Z 2016 *Mat. Res. Bull.* **76** 216
- [5] Ślebarski A, Maple M B, Wrona A, Jezierski A, Chiuzbaiian S and Neumann M 2000 *Phys. Rev. B* **62** 5
- [6] Galanakis I, Dederichs P H and Papanikolaou N 2002 *Phys. Rev. B* **66** 174429
- [7] Jezierski A and Ślebarski A 2001 *J. Magn. Magn. Mater.* **223** 33
- [8] Dordevic S V, Basov D N, Ślebarski A, Maple M B and Degiorgi L 2002 *Phys. Rev. B* **66** 075122
- [9] Chatterjee S, Das S, Pramanick S, Chatterjee S, Giri S, Banerjee A and Majumdar S 2019 *J. Magn. Magn. Mater* **478** 155
- [10] Alijani V, Ouardi S, Fecher G H, Winterlik J, Naghavi S S, Kozina X, Stryganyuk G, Felser C, Ikenaga E, Yamashita Y, Ueda S, and Kobayashi K 2011 *Phys. Rev. B* **84** 224416
- [11] Bainsla L and Suresh K G 2016 *Appl. Phys. Rev.* **3** 031101
- [12] Enamullah, Venkateswara Y, Gupta S, Varma M R, Singh P, Suresh K G and Alam A 2015 *Phys. Rev. B* **92** 224413
- [13] Bainsla L, Suresh K G, Nigam A K, Raja M M, Varaprasad B, Takahashi Y K and Hono K 2015 *Phys. Rev. B* **91** 104408
- [14] Bainsla L, Mallick A I, Raja M M, Coelho A A, Nigam A K, Johnson D D, Alam A, and Suresh K G 2015 *Phys. Rev. B* **92** 045201
- [15] Wrona A, Ślebarski A, Jezierski A, Zygmunt A, Plogmann S, Neumann M 2000 *J. Magn. Magn. Mater* **213** 157
- [16] Ślebarski A, Maple M B, Wrona A, Winiarska A 2001 *Phys. Rev. B* **63** 214416
- [17] Griffiths R B 1969 *Phys. Rev. Lett.* **23** 17
- [18] Bray A J and Moore M A 1982 *J. Phys. C: Solid State Phys*
- [19] Bray A J 1987 *Phys. Rev. Lett.* **59** 586
- [20] Salamon M B, Lin P, and Chun S H 2002 *Phys. Rev. Lett.* **88** 197203
- [21] Chatterjee A, Indra A, Gutowski O, Zimmerman M v, Majumdar S and Giri S 2021 *J. Phys.: Condens. Matter* **33** 195701
- [22] Guo S, Young D P, Macaluso R T, Browne D A, Henderson N L, Chan J Y, Henry L L and DiTusa J F 2008

- Phys. Rev. Lett* **100** 017209
- [23] Pramanik A K and Banerjee A 2010 *Phys. Rev. B* **81** 024431
- [24] Nasir M, Khan M, Agbo S A, Bhatt S, Kumar S and Sen S 2020 *J. Phys. D: Appl. Phys.* **53** 375003
- [25] Pal A, Singh P, Gangwar V K, Joshi A G, Khuntia P, Dwivedi G D, Gupta P K, Alam M, Anand K, Sethupathi K, Ghosh A K and Chatterjee S 2020 *J. Phys.: Condens. Matter* **32** 215801
- [26] Karmakar A, Majumdar S, Kundu S, Nath T K and Giri S 2012 *J. Phys.: Condens. Matter* **24** 126003
- [27] Karmakar A, Majumdar S, Kundu S, Nath T K and Giri S 2013 *J. Phys.: Condens. Matter* **25** 066006
- [28] Ghosh K, Mazumdar C, Ranganathan R, Mukherjee S and Raychaudhury M D 2018 *Phys. Rev. B* **98** 184419
- [29] Ghosh K, Mazumdar C, Ranganathan R and Mukherjee S 2015 *Sci. Rept.* **5**:15801
- [30] Magen C, Algarabel P A, Morellon L, Araujo J P, Ritter C, Ibarra M R, Pereira A M and Sousa J B 2006 *Phys. Rev. Lett.* **96** 167201
- [31] Pérez N, Casanova F, Bartolomé F, García L M, Labarta A and Batlle X 2011 *Phys. Rev. B* **83** 184411
- [32] <http://maud.radiographema.eu>
- [33] Liao Y, Practical Electron Microscopy and Database, <https://www.globalsino.com/EM/page2513.html>
- [34] Gao Q, Xie H-H, Li L, Lei G, Deng J-B and Hu X-Ru 2015 *Superlattices and Microstruct.* **85** 536
- [35] Rasool M N, Hussain A, Javed A, Khan M A and Iqbal F 2016 *Mater. Chem. Phys.* **183** 524
- [36] Greenwood N N and Gibb T C 1971 *Mössbauer Spectroscopy* (London: Chapman and Hall)
- [37] Zhang H-g, Xie L, Li Y-t, Dong X-g and Li Q J 2015 *Low Temp Phys* **178** 1
- [38] Arrot A 1957 *Phys. Rev. B* **108** 1394
- [39] Eremina R M, Fazlizhanov I I, Yatsyk I V, Sharipov K R, Pyataev A V, von Nidda H-A Krug, Pascher N, Loidl A, Glazyrin K V and Mukovskii Ya M 2011 *Phys. Rev. B* **84** 064410
- [40] Kumar J, Panja S N, Dengre S and Nair S 2017 *Phys. Rev. B* **95** 054401
- [41] Mukherjee K and Banerjee A 2009 *J. Phys.: Condens. Matter* **21** 106001
- [42] Deisenhofer J, Braak D, von Nidda H-A Krug, Hemberger J, Eremina R M, Ivanshin V A, Balbashov A M, Jug G, Loidl A, Kimura T and Tokura Y 2005 *Phys. Rev. Lett.* **95** 257202
- [43] Burgy J, Mayr M, Martin-Mayor V, Moreo A and Dagotto E 2001 *Phys. Rev. Lett.* **87** 277202
- [44] Yadav K, Sharma M K, Singh S and Mukherjee K 2019 *Sci. Rept.* **9**:15888
- [45] Galitski V M, Kaminski A, Sarma S D 2004 *Phys. Rev. Lett.* **92** 177203
- [46] Ying Y, Eom T W, Dai N V, Lee Y P 2011 *J. Magn. Magn. Mater* **323** 94
- [47] Nag R, Sarkar B, Pal S 2018 *J. Alloys Compd* **749** 385
- [48] Wang R, Gebretsadik A, Ubaid-Kassis S, Schroeder A, Vojta T, Baker P J, Pratt F L, Blundell S J, Lancaster T, Franke I, Möller J S and Page K 2017 *Phys. Rev. Lett.* **118** 267202
- [49] Castro Neto A H and Jones B A 2000 *Phys. Rev. B* **62** 14975
- [50] Naka T, Sato K, Taguchi M, Nakane T, Ishikawa F, Yamada Y, Takaesu Y, Nakama T and Matsushita A 2012 *Phys. Rev. B* **85** 085130
- [51] Ubaid-Kassis S, Vojta T and Schroeder A 2010 *Phys. Rev. Lett.* **104** 066402.
- [52] Sun Y, Salamon M B, Garnier K and Averback R S 2003 *Phys. Rev. Lett.* **91** 167206
- [53] Jonason K, Vincent E, Hammann J, Bouchaud J P and Nordblad P 1998 *Phys. Rev. Lett.* **81** 3243
- [54] Mathieu R, Jönsson P, Nam D N H and Nordblad P 2001 *Phys. Rev. B* **63** 092401.
- [55] Randeria M, Sethna J P and Palmer R G 1985 *Phys. Rev. Lett.* **54** 1321
- [56] Bray A J 1988 *Phys. Rev. Lett.* **60** 720
- [57] Das D, Das S, Singha P, Malik K, Deb A K, Bhattacharyya A, Kulbachinskii V A, Basu R, Dhara S, Bandyopadhyay S and Banerjee A 2017 *Phys. Rev. B* **96** 064116
- [58] Bessas D, Sergueev I, Wille H C, Perþon J, Ebling D and Hermann R P 2012 *Phys. Rev. B* **86** 224301
- [59] Cezairliyan A 1988 *Specific Heat of Solids (Hemisphere Pub. Corp., New York)*
- [60] Mondal S, Mazumdar C, Ranganathan R, Alleno E, Sreeparvathy P C, Kanchana V, Vaitheeswaran G 2018 *Phys. Rev. B* **98** 205130
- [61] Chaudhuri S, Salas D, Srihari V, Welter E, Karaman I and Bhohe P A 2021 *Sci. Rept.* **11** 1
- [62] Sampathkumaran E V, Mohapatra N, Rayaprol S and Iyer K K 2007 *Phys. Rev. B* **75** 052412
- [63] Lu C L, Wang K F, Dong S, Wan J G, Liu J-M and Ren Z F 2008 *J. Appl. Phys.* **103** 07F714
- [64] Venkateswara Y, Gupta S, Samatham S S, Varma M R, Enamullah, Suresh K G and Alam A 2018 *Phys. Rev. B* **97** 054407
- [65] Gnida D, Ciesielski K and Kaczorowski D 2021 *Phys. Rev. B* **103** 174206
- [66] Faber T and Ziman J 1965 *Philos. Mag.* **11** 153
- [67] Cote P J and Meisel I V 1978 *Phys. Rev. Lett.* **40** 1586
- [68] Cote P 1976 *Solid State Commun.* **18** 1311
- [69] Mizutani U, Tanaka M and Sato H 1987 *J. Phys. F. Met. Phys.* **17** 131
- [70] Harris R, Shalmon M and Zuckermann M 1978 *Phys. Rev. B* **18** 5906
- [71] Kondo J 1964 *Prog. Theor. Phys.* **32** 37
- [72] Lue C S, Ross Jr J H, Chang C F and Yang H D 1999 *Phys. Rev. B* **60** R13 941
- [73] Lue C S and Kuo Y-K 2002 *Phys. Rev. B* **66** 085121
- [74] Kuo C N, Lee H W, Wei C-M, Lin Y H, Kuo Y K and Lue C S 2016 *Phys. Rev. B* **94** 205116
- [75] Garmroudi F, Riss A, Parzer M, Reumann N, Müller H, Bauer E, Khmelevskiy S, Podloucky R, Mori T, Tobita K, Katsura Y, Kimura K 2021 *Phys. Rev. B* **103** 085202
- [76] Pallecchi I, Pani M, Ricci F, Lemal S, Bilc D I, Ghosez P, Bernini C, Ardoino N, Lamura G, Marré D 2018 *Phys. Rev. Mat.* **2** 075403
- [77] Popiel E S, Zarek W and Tuszyński M 1989 *Hyperfine Interactions* **51** 981
- [78] Popiel E S, Tuszyński M, Zarek W and Rendecki T 1989 *J. Less-Common Metals* **146** 127
- [79] Paulose P L, Mohapatra N and Sampathkumaran E V 2008 *Phys. Rev. B* **77** 172403
- [80] Jartych E, Pikula T, Garbarz-Glos B, Panek R 2018 *Acta Phys. Pol. A* **134** 1058
- [81] Marcano N, Algarabel P A, Barquín L F, Araujo J P, Pereira A M, Belo J H, Magén C, Morellón L and Ibarra M R 2019 *Phys. Rev. B* **99** 054419

- [82] Manuel P, Chapon L C, Radaelli P G, Zheng H and Mitchell J F 2009 *Phys. Rev. Lett.* **103** 037202
- [83] Karimian N and Ahmadian F 2015 *Solid State Commun.* **223** 60
- [84] Ślebarski A, Goraus J and Fijałkowski M 2011 *Phys. Rev. B* **84** 075154
- [85] Ouyang Z W, Xia N M, Wu Y Y, Sheng S S, Chen J, Xia Z C, Li L and Rao G H 2011 *Phys. Rev. B* **84** 054435
- [86] Regnat A, Bauer A, Senyshyn A, Meven M, Hradil K, Jorba P, Nemkovski K, Pedersen B, Georgii R, Gottlieb-Schönmeyer S and Pfeleiderer C 2018 *Phys. Rev. Mat.* **2** 054413
- [87] Meshcheriakova O, Chadov S, Nayak A K, Röβler U K, Kübler J, André G, Tsirlin A A, Kiss J, Hausdorf S, Kalache A, Schnelle W, Nicklas M and Felser C 2014 *Phys.Rev.Lett.* **113** 087203
- [88] Ślebarski A 2006 *J. Phys. D: Appl. Phys.* **39** 856
- [89] Snyder G and Toberer E 2008 *Nat. Mat.* **7** 105
- [90] Carr W D and Morelli D T 2015 *J. Alloys Compd.* **630** 277